https://doi.org/10.48048/tis.2022.2872

Computational Evaluation on Molecular Structure, Charge, NMR, Electronic (HOMO-LUMO) Properties, and Spectroscopic Profiling of Pioglitazone with Molecular Docking Studies

Soundhariya Segar[1,*], Keerthana Ravikumar[1], Jayasheela[2] and Periandy Sengeny[1]

[1]Department of Physics, Kanchi Mamunivar Government Institute for Post Graduate Studies and Research, Pondicherry University, Puducherry, India
[2]Department of Physics, Raak Arts and Science College, Puducherry, India

([*]Corresponding author's e-mail: soundhariyasoundhariya3949@gmail.com)

Received: 25 February 2022, Revised: 25 April 2022, Accepted: 2 May 2022, Published: 11 November 2022

Abstract

The conformational study (PES-Potential Energy Scan) has been performed and a minimum energy conformer structure has been chosen for DFT (Density Functional Theory) exploration on Pioglitazone. Extensive quantum chemical calculations have been carried out to investigate the Fourier Transform Infrared (FTIR), Fourier Transform Raman (FT-RAMAN) investigation have been implemented by emerging DFT calculations based on the B3LYP level with 6-311 ++ G (d, p) basis set, which also helps to provide useful information about the structure of the title compound. The theoretical vibrational wavenumbers are compared with the experimental values. Natural bond orbital analysis has been carried out to explain the charge transfer (or) delocalization of charge due to the intra molecular interactions. NMR has been carried through the same method along with the GIAO method for assigning ^{1}H and ^{13}C chemical shifts. UV–Visible analysis has been done by taking DMSO as a solvent to obtain maximum absorption wavelength. Mulliken atomic charges and Natural population analysis to know electronegative and electropositive atoms in a molecule. Thus, this present study reports the structural, electrical, chemical, and biological activities of Pioglitazone. The molecular docking studies revealed that the title molecule can bind with the protein 1H5U a potential antidiabetic drug.

Keywords: Pioglitazone, HDL, NBO, NMR, Glycogen, Molecular docking, Antidiabetic agent

Introduction

Pioglitazone is an antidiabetic drug used to treat type 2 diabetes mellitus, comes under thiazolidinediones which also include rosiglitazone and troglitazone [1-3]. In 1999 united states first approved pioglitazone and the European union in 2000 [4] for the treatment of diabetics. The IUPAC name of pioglitazone is 5-({4-[2-(5-ethyl pyridine-2-yl)ethoxy]phenyl}methyl)-1,3-thiazolidine-2,4-dione and the molecular formula is $C_{19}H_{20}N_2O_3S$. It is administrated orally: insoluble in water and ether: slightly soluble in acetone, acetonitrile, and alcohol; soluble in dimethylformamide (DMF) and dimethyl sulfoxide (DMSO) [1,4]. Type 2 diabetes is mainly due to lifestyle changes and it's a chronic disease particularly high among South Asians [4]. Pioglitazone is used, to control high blood sugar, sometimes in combination with other diabetes medications such as sulfonylurea, metformin or, insulin. It helps the body to restore proper response to insulin by lowering blood sugar and kidney damage, blindness, nerve problems, loss of limbs, and proper control of diabetes lessen the risk of heart attack or stroke [5]. This drug is used indirectly to increase high–density lipoproteins (HDL) without changing low-density lipoproteins (LDL) [4,5].

It was also noted that pioglitazone works through a unique mechanism of action of insulin sensitization and beta-cell preservation and decreases HbA1C (Hemoglobin A1C) levels during 8 weeks of treatment and the maximum benefit at 16 weeks of treatment [4,5]. Pioglitazone also has antidepressant properties [1,4]. Since diabetes is a metabolic disease occurring when the pancreas does not produce enough insulin, Pioglitazone acts through the nuclear hormone, peroxisome proliferator-activated receptor-gamma (PPARϒ) which increases insulin sensitivity by enhancing the expression of proteins responsible for modulating glucose and lipid metabolism leading to improved insulin sensitivity in the liver, muscle and adipose tissue [6,7]. Since insulin is the hormone that stimulates cells to remove glucose from the blood, the reduced amount of insulin and its reduced effect cause cells to take up less glucose from the blood and the level of glucose in the blood to rise. Pioglitazone often is referred to as an "insulin

sensitizer" because it attaches to the insulin receptors on cells throughout the body and causes the cells to become more sensitive to insulin [8-10].

The literature survey shows that DFT studies particularly combined with experimental spectroscopic analysis is not done so far, hence the present work is undertaken to thoroughly study the structural, vibrational, NBO, NMR, HOMO-LUMO, and UV-Vis properties and behavior of the molecule to reveal more insight into the physicochemical mechanism.

Materials and methods

Experimental details

The compound Pioglitazone was purchased in commercial tablet form and the FT-IR spectrum was recorded in Bruker IFS 66V spectrometer in the range of 4000 - 500 cm^{-1}. The spectral resolution is ±2 cm^{-1} and the FT-Raman spectrum of compound was also recorded in the same instrument with FRA 106 Raman module equipped with Nd: YAG laser source operating at 1.064 µm line widths with 200 mW power in the range of 4000 - 400 cm^{-1} with a scanning speed of 30 cm^{-1} $min^{-1}$and spectral width 2 cm^{-1}. The frequencies of all bands are accurate to ±1 cm^{-1}. The UV-Vis spectra were recorded in the liquid phase dissolved in ethanol in the range of 200 to 400 nm, with the scanning interval of 0.5 nm, using the UV-1700 series instrument.

Computational details

All the quantum chemical computations in the present work are performed using the Gaussian 09 software programs on a Pentium IV/3.02GHz personal computer [11]. The geometrical parameters were computed using B3LYP functional with a 6-311++G (d, p) basis set [12-15]. The UV-Visible spectrum, electronic transition such as HOMO-LUMO excitation energy, and oscillator strength were calculated using the time-dependent TD-SCF-B3LYP method. The NMR chemical shift was carried out by the GIAO method along with B3LYP and 6-311G++ (d, p) basis set. The natural bonding orbital (NBO) computations were done at the B3LYP/6-311++G (d, p) level using second-order perturbation theory. In addition, the dipole moment, linear polarizability, and the first-order hyperpolarizability of the title molecule are also computed using the B3LYP method and 6-311++G (d, p) basis set.

Result and discussions

Conformational analysis

A potential energy surface scan using the B3LYP level and the quantum approach was used to identify conformers for the molecule. The B3LYP/6-311++G (d, p) hybrid functional was used to investigate the energy changes caused by pioglitazone rotation around bonds. The numerous spatial configurations gained by rotating the molecule around sigma bonds indicate conformations [16,17]. Because the spatial arrangement of atoms in a molecule has a substantial influence on all molecular properties, as well as the outcome of chemical reactions, knowing the forces involved in the work and energy of processes is vital. This scan was performed to minimize the energy level of all geometrical parameters with the change of torsional angle C10-C1-C5-N9 is rotated through 360° in the step of 10° for obtaining the respective conformers of the compound through a complete rotation around the bond. The graphical result is shown in **Figure 1**. Two minimum energy conformers were acquired at 164° and 311° with their energies at −0.141Hartree. This represents the stable conformer of the compound.

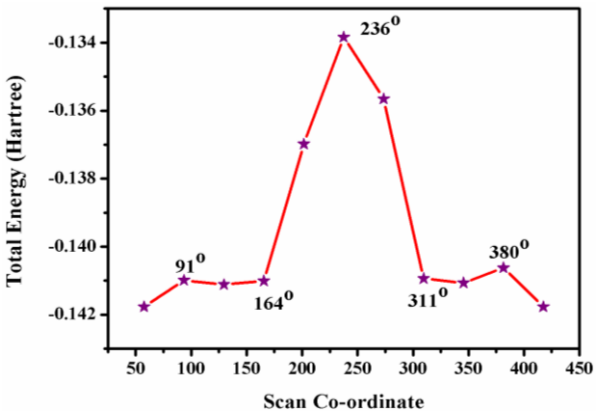

Figure 1 Conformational analysis of Pioglitazone.

Structural analysis

The calculated bond length, bond angle, and dihedral angle using B3LYP functional and 6-311++G (d, p) basis sets for Pioglitazone with experimental values are calculated, and the structure of the compound in the optimized form are shown in **Figure 2**. The CC bond lengths of the aromatic ring are expected either 1.39 or 1.38 Å, in the present molecule, as shown in the table 1, the phenyl ring has values of 1.40 Å, in addition to 1.38 & 1.39 Å. A small increase in the value is observed to be due to the O atom in the ethoxy group attached at C13 and the thiazole group at C17. In the case of the pyridine ring, all the CC values are identical and found to be 1.39Å, the 2 CN values are 1.34 and 1.33 Å, which is in agreement with reference value [18,19] that shows there is also a conjugation pattern inside the pyridine ring like in phenyl ring.

The pyridine ring shows no influence of other groups in the molecule. In the case of the ethyl group, the 2 CC are found to have lengths equal to 1.51 and 1.53 Å, the first one is attached with pyridine which might be the influence, for shortening of the bond. In methoxy, the CC value is 1.52 Å, so all these CC values in the aliphatic chain are purely single bonded and show no trace of any kind of conjugation. In the thiazolidine group, there is only one CC whose value is found to be 1.53 Å, which shows it is also exactly behaving like an aliphatic chain rather than as a ring. Among the CN bonds in the thiazolidine ring, C21-N23 is 1.38 and C22-N23 is 1.39, these 2 values are also purely single-bonded which being unlike confirms the conjugation present in the pyridine ring. The (CS) bond length is expected to be around 1.70 Å whereas the observed C20-S27 and C22-S27 bond length values are 1.84 and 1.79 Å which is higher than the expected range. This may be due to the influence of 2 double bonded oxygen atoms attached to the thiazole ring.

All the bond angles around C are expected to be either 120 or 109 degree due to sp^2 or sp^3 hybridizations, but within the pyridine rings some of the angles C3-C4-N9 (121º), C3-C4-C11 (121º), and N9-C4-C11 (116º) are found to deviate these values, this is naturally due to the presence of N atom in the ring, which disturbs the electronic distribution in the ring and hence the hybridization of the carbon atoms in the ring. Similarly, in the case of thiazolidine ring; C19-C20-C21 (111º), C19-C20-S27 (113º), C21-C20-S27 (106º), C20-C21-N23 (111º), C20-C21-O25 (124º), N23-C21-O25 (124º), and N23-C22-O24 (125º). All these values create the distortion of the hybridization and hence bond angles from the expected values.

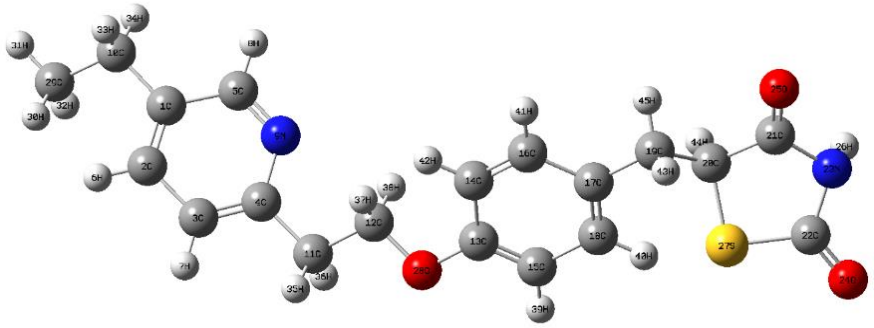

Figure 2 Molecular structure of Pioglitazone (5-({4-[2-(5-ethylpyridin-2-yl)ethoxy]phenyl}methyl)-1,3-thiazolidine-2,4-dione).

Table 1 Optimized geometrical parameter for Pioglitazone computed at B3LYP/6-311++G (d, p).

Bond Length (Å)	B3LYP/ 6-311++G (d,p)	Bond Angle (◦)	B3LYP/ 6-311++G (d, p)	Dihedral Angle (◦)	B3LYP/ 6-311++G (d, p)
C1-C2	1.3959	C2-C1-C5	116.3054	C5-C1-C2-C3	−0.1747
C1-C5	1.3989	C2-C1-C10	122.3037	C5-C1-C2-H6	179.4401
C1-C10	1.5105	C5-C1-C10	121.3784	C10-C1-C2-C3	178.5546
C2-C3	1.3908	C1-C2-C3	119.8114	C10-C1-C2-H6	−1.8306
C2-H6	1.0859	C1-C2-H6	120.1593	C2-C1-C5-H8	−179.344
C3-C4	1.3976	C3-C2-H6	120.0281	C2-C1-C5-N9	0.1072

Bond Length (Å)	**B3LYP/ 6-311++G (d,p)**	**Bond Angle (◦)**	**B3LYP/ 6-311++G (d, p)**	**Dihedral Angle (◦)**	**B3LYP/ 6-311++G (d, p)**
C3-H7	1.0842	C2-C3-C4	119.2745	C10-C1-C5-H8	1.9136
C4-N9	1.3409	C2-C3-H7	120.5975	C10-C1-C5-N9	−178.635
C4-C11	1.5114	C4-C3-H7	120.1257	C2-C1-C10-C29	−83.5465
C5-H8	1.0883	C3-C4-N9	121.508	C2-C1-C10-H33	38.4966
C5-N9	1.3339	C3-C4-C11	121.9318	C2-C1-C10-H34	154.5711
C10-C29	1.5388	N9-C4-C11	116.5601	C5-C1-C10-C29	95.1192
C10-H33	1.0949	C1-C5-H8	119.649	C5-C1-C10-H33	−142.838
C10-H34	1.0945	C1-C5-N9	124.6111	C5-C1-C10-H34	−26.7632
C11-C12	1.5254	H8-C5-N9	115.7378	C1-C2-C3-C4	0.2004
C11-H35	1.0940	C4-N9-C5	118.4892	C1-C2-C3-H7	179.6586
C11-H36	1.0926	C1-C10-C29	113.0989	H6-C2-C3-C4	−179.415
C12-O28	1.4300	C1-C10-H33	109.324	H6-C2-C3-H7	0.0433
C12-H37	1.0941	C1-C10-H34	109.1932	C2-C3-C4-N9	−0.152
C12-H38	1.0972	C29-C10-H33	109.3117	C2-C3-C4-C11	179.7609
C13-C14	1.3982	C29-C10-H34	109.2598	H7-C3-C4-N9	−179.613
C13-C15	1.4000	H33-C10-H34	106.4353	H7-C3-C4-C11	0.3001
C13-O28	1.3626	C4-C11-C12	111.6437	C3-C4-N9-C5	0.0793
C14-C16	1.3953	C4-C11-H35	109.26	C11-C4-N9-C5	−179.838
C14-H42	1.0815	C4-C11-H36	110.4405	C3-C4-C11-C12	117.0591
C15-C18	1.3874	C12-C11-H35	108.2877	C3-C4-C11-H35	−123.188
C15-H39	1.0834	C12-C11-H36	109.393	C3-C4-C11-H36	−4.8876
C16-C17	1.3955	H35-C11-H36	107.7092	N9-C4-C11-C12	−63.0239
C16-H41	1.086	C11-C12-O28	107.368	N9-C4-C11-H35	56.7287
C17-C18	1.4017	C11-C12-H37	109.8643	N9-C4-C11-H36	175.0294
C17-C19	1.512	C11-C12-H38	110.6616	C1-C5-N9-C4	−0.0592
C18-H40	1.0849	O28-C12-H37	110.3893	H8-C5-N9-C4	179.4116
C19-C20	1.5439	O28-C12-H38	109.7827	C1-C10-C29-H30	59.7617
C19-H43	1.0934	H37-C12-H38	108.7716	C1-C10-C29-H31	179.8344
C19-H45	1.094	C14-C13-C15	119.3549	C1-C10-C29-H32	−60.0826
C20-C21	1.53	C14-C13-O28	124.6533	H33-C10-C29-H30	−62.2884
C20-S27	1.8488	C15-C13-O28	115.991	H33-C10-C29-H31	57.7843
C20-H44	1.0922	C13-C14-C16	119.5813	H33-C10-C29-H32	177.8673
C21-N23	1.3811	C13-C14-H42	121.0604	H34-C10-C29-H30	−178.393
C21-O25	1.2083	C16-C14-H2	119.3548	H34-C10-C29-H31	−58.3205
C22-N23	1.3935	C13-C15-C18	120.2202	H34-C10-C29-H32	61.7625
C22-O24	1.2008	C13-C15-H39	118.6469	C4-C11-C12-O28	177.8416
C22-S27	1.7941	C18-C15-H39	121.132	C4-C11-C12-H37	57.7666

Bond Length (Å)	**B3LYP/ 6-311++G (d,p)**	**Bond Angle (◦)**	**B3LYP/ 6-311++G (d, p)**	**Dihedral Angle (◦)**	**B3LYP/ 6-311++G (d, p)**
N23-H26	1.0128	C14-C16-C17	121.7634	C4-C11-C12-H38	−62.3604
S27-H40	3.3907	C14-C16-H41	118.5905	H35-C11-C12-O28	57.5175
C29-H30	1.0935	C17-C16-H41	119.6424	H35-C11-C12-H37	−62.5576
C29-H31	1.0934	C16-C17-C18	117.7793	H35-C11-C12-H38	177.3155
C29-H32	1.0933	C16-C17-C19	120.8166	H36-C11-C12-O28	−59.6101
		C18-C17-C19	121.4029	H36-C11-C12-H37	−179.685
		C15-C18-C17	121.2996	H36-C11-C12-H38	60.1879
		C15-C18-H40	119.0784	C11-C12-O28-C13	−179.156
		C17-C18-H40	119.6216	H37-C12-O28-C13	−59.4151
		C17-C19-C20	113.6274	H38-C12-O28-C13	60.4873
		C17-C19-H43	110.3287	C15-C13-C14-C16	0.1883
		C17-C19-H45	110.2211	C15-C13-C14-H42	−179.126
		C20-C19-H43	108.8352	O28-C13-C14-C16	179.834
		C20-C19-H45	106.4074	O28-C13-C14-H42	0.5194
		H43-C19-H45	107.1533	C14-C13-C15-C18	−0.194
		C19-C20-C21	111.3678	C14-C13-C15-H39	179.4751
		C19-C20-S27	113.9716	O28-C13-C15-C18	−179.87
		C19-C20-H44	109.4523	O28-C13-C15-H39	−0.2006
		C21-C20-S27	106.7663	C14-C13-O28-C12	−0.0086
		C21-C20-H44	107.2485	C15-C13-O28-C12	179.6479
		S27-C20-H44	107.7508	C13-C14-C16-C17	0.1018
		C20-C21-N23	111.3951	C13-C14-C16-H41	−179.189
		C20-C21-O25	124.1832	H42-C14-C16-C17	179.4283
		N23-C21-O25	124.4203	H42-C14-C16-H41	0.1372
		N23-C22-O24	125.0546	C13-C15-C18-C17	−0.0904
		N23-C22-S27	109.4468	C13-C15-C18-H40	179.6706
		O24-C22-S27	125.4986	H39-C15-C18-C17	−179.751
		C21-N23-C22	119.6414	H39-C15-C18-H40	0.0098
		C21-N23-H26	120.8177	C14-C16-C17-C18	−0.376
		C22-N23-H26	119.5408	C14-C16-C17-C19	179.2364
		C20-S27-C22	92.7455	H41-C16-C17-C18	178.9078
		C12-O28-C13	118.9572	H41-C16-C17-C19	−1.4798
		C10-C29-H30	111.1455	C16-C17-C18-C15	0.3696
		C10-C29-H31	110.8018	C16-C17-C18-H40	−179.39
		C10-C29-H32	111.0069	C19-C17-C18-C15	−179.24
		H30-C29-H31	107.9858	C19-C17-C18-H40	0.9999
		H30-C29-H32	107.6963	C16-C17-C19-C20	−82.3962

Bond Length (Å)	B3LYP/ 6-311++G (d,p)	Bond Angle (◦)	B3LYP/ 6-311++G (d, p)	Dihedral Angle (◦)	B3LYP/ 6-311++G (d, p)
		H31-C29-H32	108.0669	C16-C17-C19-H43	155.0656
				C16-C17-C19-H45	36.9246
				C18-C17-C19-C20	97.2021
				C18-C17-C19-H43	−25.3362
				C18-C17-C19-H45	−143.477
				C17-C19-C20-C21	171.9503
				C17-C19-C20-S27	−67.1883
				C17-C19-C20-H44	53.535
				H43-C19-C20-C21	−64.6917
				H43-C19-C20-S27	56.1697
				H43-C19-C20-H44	176.893
				H45-C19-C20-C21	50.4772
				H45-C19-C20-S27	171.3386
				H45-C19-C20-H44	−67.9381
				C19-C20-C21-N23	124.2738
				C19-C20-C21-O25	−55.2989
				S27-C20-C21-N23	−0.7219
				S27-C20-C21-O25	179.7054
				H44-C20-C21-N23	−115.996
				H44-C20-C21-O25	64.4313
				C19-C20-S27-C22	−122.783
				C21-C20-S27-C22	0.6117
				H44-C20-S27-C22	115.5477
				C20-C21-N23-C22	0.5073
				C20-C21-N23-H26	−179.631
				O25-C21-N23-C22	−179.921
				O25-C21-N23-H26	−0.0598
				O24-C22-N23-C21	179.9265
				O24-C22-N23-H26	0.0634
				S27-C22-N23-C21	−0.0143
				S27-C22-N23-H26	−179.878
				N23-C22-S27-C20	−0.3728
				O24-C22-S27-C20	179.6867

Mulliken and natural atomic charges

Prediction of atomic charges plays an important role in understanding the properties of the molecule as the atomic charges cause the dipole moment, polarizability, bond strength, bond angles, vibrational wavenumbers, electronic transition, and molecular reactivity of the system. The charges on the atoms of the present compound are calculated by 2 methods; Mulliken Population analysis (MPA) method and natural atomic charge (NAC) method comparison, using B3LYP method with 6-311++ G (d, p) basis set, the values are presented and the graphical representation of the same is presented in **Figure 3**.

In the case of the phenyl ring, all the carbon atoms are expected to be equally negative, in the present case, the carbon atoms show interesting results in their polarity observed Mulliken and NAC. The change of charge polarity implies the high flow of charge within the ring. The charges on all the carbon atoms the phenyl are as expected, except at C17 and C13, on carbon C17 where the thiazolidine ring is substituted, it is highly positive in MPA and almost neutral or slightly negative (−0.04769). In this case, the logic used in MPA may not be correct, as thiazolidine cannot draw a huge amount of charge from phenyl, hence it can only be less negative as predicted by NAC [20,21]. At C13 where the oxygen atom of the ethoxy group is attached, it is highly positive in NAC (0.31124) but usually negative (-0.12822) in MPA, again in this case also the MPA prediction may not be correct as the O atom is highly electronegative.

In the case of carbon atoms in the pyridine ring, all carbon atoms are found to equally be negative as expected for phenyl, except at C1, C4, and C5. At C1 where the ethyl group is substituted, it is found to be highly positive (1.001) in MPA and slightly negative in NAC (−0.059). As the ethyl group is almost neutral, it cannot draw many electrons from pyridine, hence it cannot be highly positive as shown by MPA. C4 and C5 are adjacent atoms in the ring, besides at C4 the ethoxy group is attached, hence it is shown to be highly positive in both the methods (0.114 in MPA and 0.177 in NAC). At C5, it is shown to be highly negative in MPA (−0.415) and moderately positive in NAC (0.109), even in this case only the prediction of NAC can be true, as the electron pulling power of the N atom is shared by both these carbon atom.

In the thiazolidine ring, 2 carbon atoms C21 and C22 are attached O atoms with double-bond and they also lie adjacent to N atom, both are predicted to be negative in MPA (−0.57802 & −0.20762) but highly positive in NAC (0.7146 &0.49656). Here also the prediction by MPA cannot be true as they are connected to 2 highly electronegative atoms. C20 is connected to a methyl group and S atom, which is predicted to be highly positive (0.66376) in MPA and highly negative (−0.43303) in NAC in this case, both the methods may be wrong, as there is a possibility for less positive or neutral.

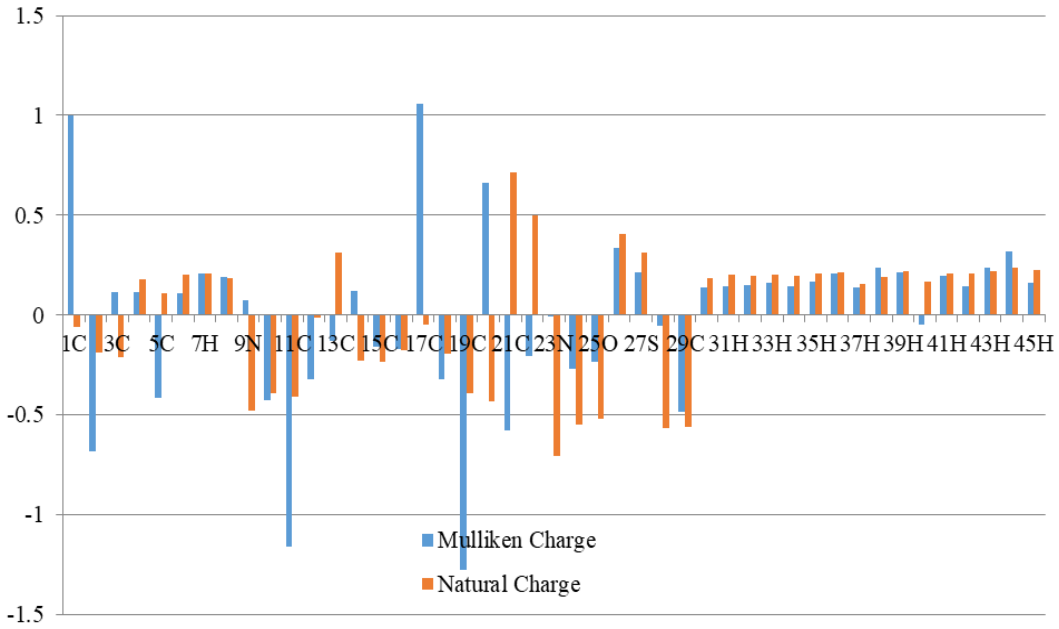

Figure 3 Charge analysis of Pioglitazone.

Nuclear magnetic resonance (NMR) analysis

The optimized structure of Pioglitazone was used to calculate the NMR chemical shift at B3LYP levels in combination with GIAO methods and 6- 311++G (d, p) basis set. The ^{1}H and ^{13}C chemical shifts computed in ppm (parts per million) relative to TMS are shown in **Table 2**, and **Figure 4**. The chemical shifts were computed for both gas and $CDCl_3$ (Deuterated chloroform) solvent phases and discussion is held for the solvent phases as the experimental value are recorded in the solvent phase only.

The carbon atoms in the phenyl ring usually give chemical shift values ranging from 120 to 130 ppm [22]. The magnetic field experienced externally by the carbon nuclei is affected by the electronegativity of the atoms attached to them. Therefore, electronegative substituents attached to carbon reduce the local diamagnetic shielding in the vicinity of the attached proton and de-shield them. The greater the electronegativity of the substituent atom, the more it de-shields proton and greater is the chemical shift.

In the case of the phenyl ring in the present molecule, the chemical shift of C13 where O of the ethoxy group attached directly is found to have a maximum value of 177 ppm, whereas C17, where the thiazolidine group is attached is found to have shift 147 ppm, these 2 observation are in agreement with charges predicted by NAC methods as seen in the charge analysis. C16 and C18 are also found to have slightly enhance-shifts of 142 and 141 ppm, respectively which are in contrast to the results of the charge analysis. The other 2 carbon atoms in phenyl have values within the expected range.

In the case of carbon atoms in pyridine ring, at C1 where ethyl group is substituted, it is found to have shift 156 ppm. The carbon atoms C4 and C5 which are adjacent to the N atom in the ring, both are found to have an almost equal shift of 167 and 166 respectively. The other carbon atoms in this ring are within the expected range of 120 to 130 ppm, as in the benzene ring. All these chemical shift values by charges predicted by the NAC method.

In the thiazolidine ring, 2 carbon atoms C21 and C22 are attached O atoms with double - bond and they also lie adjacent to N atom, these are found to have maximum shifts of 177 and 175 ppm respectively, actually, their ranges should be in the level of aliphatic chain between 30 to 40 ppm, but the presence of the double-bonded O and adjacent N atom has greatly increased their shift values. Whereas C20 which is connected with a methyl group and S atom is found to have shifted only 65 ppm. All these predictions are in agreement with the discussions held in atomic charge analysis. The chemical shift values of C21 and C22 indicate that they too will play a significant role in the biological properties of the molecule. The ^{1}H NMR spectrum of the compound has 7 proton signals due to 7 different proton environments as plotted in the figure. H attached to an aromatic ring has a chemical shift from 7-8 ppm [23]. The ring hydrogen atoms 8H, 40H, 42H in the compound are assigned to the chemical shift value are very greater in between 8 - 10 ppm, respectively in $CDCl_3$ solution.

The NMR chemical shift for C13 in benzene ring is found at 177 ppm and that if C4 and C5 in pyridine ring at 167 and 166 ppm, respectively. High chemical shift value for carbon atoms, particularly above 150 ppm, indicate that these carbon atoms will be involved in prominent electronic transition in the molecule, which in turn determines the biological property of the molecule. The prominent electronic transitions among these carbon atoms in the molecule determined by the NBO analysis are O28 to C13 - C14 (30.15 $KJmol^{-1}$) (n-π*), C2 - C3 to C4 - N9 (27.87 $KJmol^{-1}$) (π-π*) & C4 - N9 to C1 - C5 (25.73 $KJmol^{-1}$) (π-π*).

Table 2 Calculated both ^{1}H and ^{13}C NMR chemical shifts (ppm) of Pioglitazone.

Atom	^{1}H-NMR Chemical Shift (ppm)			Atom	^{13}C-NMR Chemical Shift (ppm)	
	Gas	$CDCl_3$	Experimental		Gas	$CDCl_3$
6H	7.6323	8.0442	7.574	1C	143.748	156.919
7H	7.2434	7.3064	7.556	2C	140.671	141.161
8H	8.7197	9.2377	8.354	3C	126.422	131.771
26H	6.5914	4.5343	4.795	4C	162.935	167.837
30H	1.0008	1.0454	1.116	5C	156.028	166.898
31H	1.2558	0.5865	1.224	10C	30.1297	24.6876
32H	1.0008	0.0547	1.166	11C	41.1407	36.0601
33H	2.3303	1.9702	1.941	12C	70.8471	69.9033
34H	2.6096	2.0033	2.553	13C	166.193	177.55

Atom	^{1}H-NMR Chemical Shift (ppm)			Atom	^{13}C-NMR Chemical Shift (ppm)	
	Gas	$CDCl_3$	Experimental		Gas	$CDCl_3$
35H	3.4131	2.6691	2.501	14C	113.926	134.256
36H	2.9589	2.9177	2.967	15C	122.699	119.994
37H	4.2944	4.5811	4.539	16C	133.95	142.495
38H	3.7346	4.1132	4.675	17C	134.333	147.424
39H	7.1042	7.053	7.114	18C	135.358	141.977
40H	7.3237	10.1777	12.025	19C	43.3613	36.0996
41H	7.3124	7.6696	7.601	20C	65.9314	58.5414
42H	6.7435	8.0983	7.588	21C	177.617	213.008
43H	2.5792	2.495	2.483	22C	175.069	207.991
44H	4.0059	3.9637	3.623	29C	19.2996	10.5114
45H	3.567	3.1058	3.570			

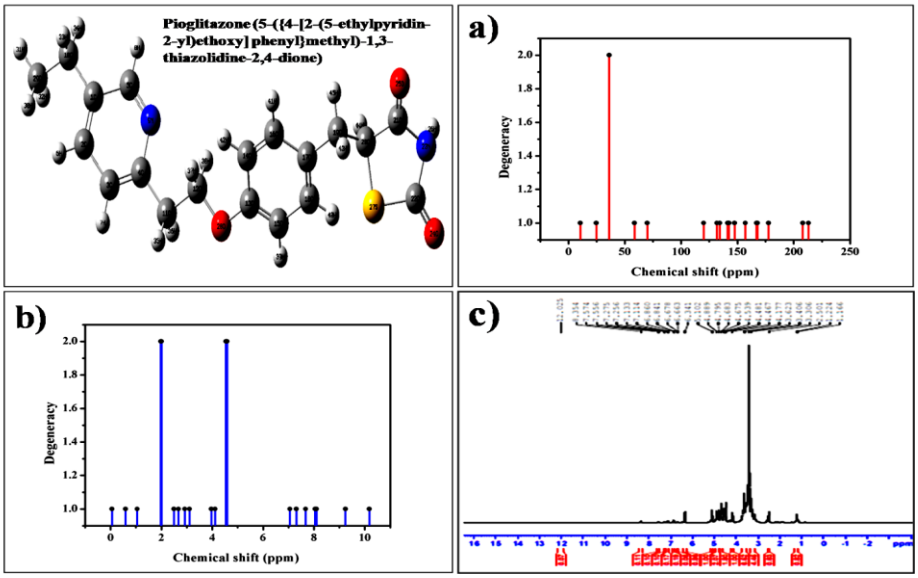

Figure 4 a), b) are theoretical ^{1}H and ^{13}C NMR, and c) experimental ^{1}H NMR spectrum of Pioglitazone.

Vibrational analysis

The title molecule has 46 atoms, belongs to C1 point group symmetry, and has 132 possible modes of vibrations. All these modes of vibrations are predicted theoretically and the corresponding modes are obtained from experimental spectra for all the prominent modes. The theoretical and experimental spectra of the compound are presented in Figure 5 and the theoretical and experimental wave numbers, along with the vibrational constants are in the discussion respectively [24,25].

CH vibrations

For the aromatic compounds the carbon-hydrogen stretching vibration is observed in the region 3100 - 3000 cm^{-1} and for aliphatic in the region 3000 - 2900 cm^{-1} [26]. In pyridine and benzene ring, there are 3 and 4 CH modes, all these 7 stretching values are expected above 3000 cm^{-1} but among the scaled values, only 4 bands 3045, 3033, 3021 and 3008 cm^{-1} are observed in this region, the remaining 3 bands are observed at 2997, 2979 and 2972 cm^{-1}, all these 3 values are very close to 3000 cm^{-1}. Hence the benzene CH stretching values are found to be slightly less than the usual aromatic values in this molecule. The only one CH stretching in the thiazole ring is observed at 2940 cm^{-1}, these is slightly less than the CH vibration in the benzene and pyridine ring which confirm the previous observation that the conjugation in the thiazole is very weak. The CH stretching vibrations in the ethoxy group are observed at

2939, 2936, 2933, 2918 cm^{-1}, these are slightly enhanced values when compared to the purely aliphatic CH values which lies usually less than 2900 cm^{-1}, which is clearly due to the presence of oxygen atom in the ethoxy group. This CH stretching vibrations for the methylene and ethyl group in the molecule are observed in between 2907 - 2851 cm^{-1}. This values are in agreement with the expected aliphatic range. Hence the influence of other rings on this groups is very small. The C-H in-plane bending mode usually occurs as strong to weak bands in the region of 1300 to 1200 cm^{-1} [27]. The C-H out-of-plane bending vibrations are expected to occur as strong to weak intensity bands in the region of 1000 - 600 cm^{-1}. In this case present molecule all the observed scaled values are lies in the expected range.

CS and NH vibrations

The C-S stretching vibration is observed at 662 cm^{-1} in the FT-IR spectrum. Similarly, the C-S stretching vibration is found at 659 and 645 cm^{-1} from the computed values [28]. The C-S in the plane and out of plane bending vibration is observed values are lies in the expected range.

The NH stretching vibration is observed at 3417 cm^{-1} in FT-IR spectra [29]. But observed scaled values at 3539 cm^{-1}. These values are slightly greater than the experimental values due to the presence of Sulfur and oxygen atoms.

CO vibrations

The stretching mode of the carbonyl (C=O) group of the ketone moiety is expected in the range of 1750 to 1730 cm^{-1} [30]. Two C=O bonds are present in the thiazole ring, whose experimental vibrations are observed at 1743 and 1603 cm^{-1}, in which 1743 cm^{-1} is in agreement with the literature value, whereas 1603 is very less, it may be due to the influence of sulphur atom attached to this C=O group. Two single bonds are present in the ethoxy group whose stretching value are observed at 1519 and 1516 cm^{-1}, these are in agreement with the literature value, hence it means these C-O modes remains unaffected by the other modes.

CC vibrations

The CC stretching modes are normally found in the region between 1600 - 1400 cm^{-1} [31,32]. In the title molecule, CC stretching vibrations were observed between 1682 - 1548 cm^{-1} in FT-Raman and a medium band was observed in between 1692 - 1460 cm^{-1} in FT-IR. The observation of all these values, for both double bond and single bond CC stretching, in comparison with the literature values show that some of the band values are higher than the expected values and some of them are lower than the expected values, there is stretching of values on both ends of the expected region, which is naturally due to Fermi resonance effect between these values.

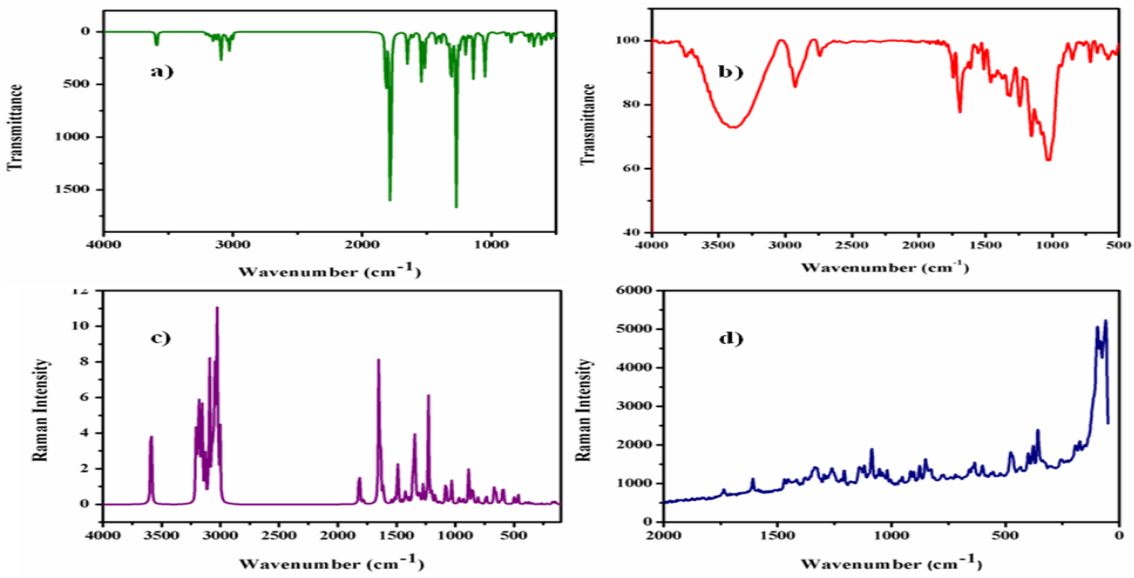

Figure 5 a), c) are theoretical FT-IR and FT-Raman spectrum and b), d) are Experimental FT-IR and FT-Raman spectrum of Pioglitazone.

Natural bonding orbital (NBO) analysis

Natural bonding orbital (NBO) analysis gives the possible natural Lewis structure of Ψ since all orbital details are chosen mathematically for including the highest possible percentage of the electron density. The analysis is an efficient method for studying intra and inter-molecular interaction among bonds and for investigating charge transfer or conjugative interaction in a molecular system. The second-order Fock matrix was carried out for evaluating the donor-acceptor interaction [33,34]. For each donor NBO (i) and acceptor NBO (j) the stabilization energy $E^{(2)}$ [35] associated with the electron delocalization i → j is estimated as:

$$E_2 = \Delta E_{ij} = q_i \frac{F(i,j)^2}{E_i - E_j}$$

The larger the $E^{(2)}$ value, the more intensive is the interaction between donors and acceptors. Parameter such as occupancy, electron donors and accepters, stabilization energy, etc., are extracted from the NBO Gaussian output by B3LYP/6-311++G (d, p) method are calculated. According to the calculation and stabilization energy values of the donor and acceptor interactions, the top most 10 possible transitions in this molecule are N23 to C22 - O24 (51.33 $KJmol^{-1}$) (n-π*), N23 to C21 - O25 (50.45 $KJmol^{-1}$) (n-π*), O24 to C22 - S27 (31.32 $KJmol^{-1}$) (n-π*), O28 to C13 - C14 (30.15 $KJmol^{-1}$) (n-π*), S27 to C22 - O24 (28.4 $KJmol^{-1}$) (n-π*), C2 - C3 to C4 - N9 (27.87 $KJmol^{-1}$) (π-π*), O25 to C21 - N23 (27.21 $KJmol^{-1}$) (n-σ*), O24 to C22 - N23 (26.2 $KJmol^{-1}$) (n-σ*), C4 - N9 to C1 - C5 (25.73 $KJmol^{-1}$) (π-π*), C1 - C5 to C2 - C3 (22.59 $KJmol^{-1}$) (π-π*). Among these 10 most probable transitions, 7 transitions (top, 5, 7^{th} and 8^{th}) are found to be the thiazolidine group which shows the n within the ring and double-bonded O outside ring contribute enormously to the electronic property of the molecule. The other 3 transitions are from the pyridine group. All the transitions in the thiazolidine group belong to n-π* transition and those in the pyridine group are π-π* transitions. However, all these probable transitions will not be found active in the experimental UV-Visible spectrum as they are restricted by selection rules, which can be also theoretically ascertained from HOMO-LUMO contribution and oscillator strength as discussed in the following section.

UV-Visible analysis

The UV-Visible spectra analysis of the compound has been studied in both DMSO and gas phases, as the experimental spectrum is recorded in the DMSO phase. The excitation energies and oscillator strengths of Pioglitazone were computed using B3LYP functional and 6-311++G (d, p) basis set along with TD–SCF method. The computed excitation energies, oscillator strength (f) and absorption wavelength (λ), and HOMO-LUMO contributions are presented below. The UV-theoretical and Experimental spectra are presented in **Figure 6**.

The computed absorption wavelength, in gas phase, are predicted to take place at 279, 269, 259, 255, 248, 247, 240, 239, 238, 233 nm with excitation energies 4.43, 4.59, 4.77, 4.85, 4.99, 5.01, 5.15, 5.18, 5.20, 5.31 eV, respectively. The HOMO-LUMO major contribution is observed for transition N23 to C22 - O24 (51.33 KJ mol^{-1}) (n-π*), with 97 % using the Gauss sum program. The oscillator strength values indicate the 7^{th} transition O25 to C21 - N23 (27.21 $KJmol^{-1}$) (n-σ*) at 240 nm will have maximum intensity among all other transitions.

Similarly, in DMSO phase, the corresponding absorption bands are observed at 281, 261, 255, 252, 244, 240, 239, 238, 235, 231 nm with excitation energies 4.39, 4.73, 4.85, 4.91, 5.07, 5.16, 5.18, 5.20, 5.26, 5.34 eV respectively. Here HOMO-LUMO major contribution is observed for transition N23 to C22 - O24 (51.33 $KJmol^{-1}$) (n-π*) as 98 % [36]. But, in this solvent phase, according to oscillator strength value, only the 6^{th} transition C2 - C3 to C4 - N9 (27.87 $KJmol^{-1}$) (π-π*) will have the maximum intensity instead of 7^{th} as seen in the gas phase. Thus, it may be concluded that solvents not only change the observable peaks in the UV-Vis spectrum, but also the wavelengths of absorption. Since the oscillator strengths are very close to almost all transitions, except 5^{th} and 10^{th}, a broad hump is expected from 235 to 280 nm in the experimental spectrum, with 3 or 4 weak peaks on the hump.

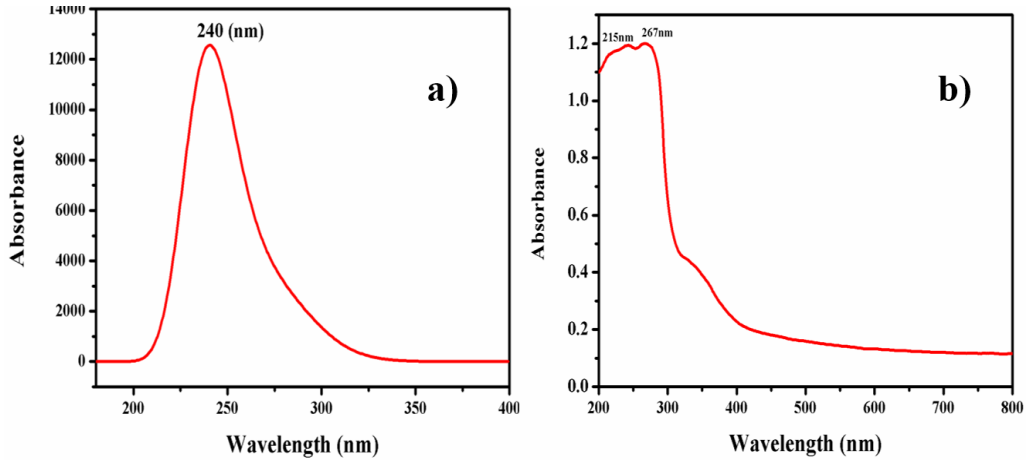

Figure 6 a) theoretical and b) experimental UV-Visible graph of Pioglitazone.

HOMO-LUMO

FMO analysis indicates the chemical stability of the molecule, HOMO represents the highest occupied molecular orbitals, and LUMO is the lowest un-occupied molecular orbitals, both of which are called Frontier molecular orbitals FMO. The difference in energy between the HOMO and LUMO is called the energy band gap. This energy gap determines the molecular electrical transport property, chemical reactivity, optical polarizability, chemical hardness, and softness of the molecule [37-39].

All these highest occupied molecule orbitals and lowest unoccupied orbitals are determined with B3LYP functional and 6-311++G (d, p) basis set and the same is shown diagrammatically in **Figure 7**. The calculated energy of HOMO is 0.256 eV and LUMO is 0.023 eV and the energy gap between them is 0.232 eV as shown in **Table 3**. The electronegativity is the measure of the attraction of electron by an atom in a covalent bond has a value of 0.1400 eV. The chemical hardness of the molecules is 0.1163 eV and softness is 0.465 eV.

Table 3 HOMO, LUMO, electronegativity, global hardness and softness, chemical potential of Pioglitazone.

Parameters	Gas
E_{HOMO} (eV)	−0.25642
E_{LUMO} (eV)	−0.02370
$\Delta E_{HOMO\text{-}LUMO\ gap}$ (eV)	−0.23272
Electronegativity (χ)	−0.14006
Global hardness (η)	−0.11636
Global softness (S)	−0.46544
Chemical Potential (μ)	−0.08429

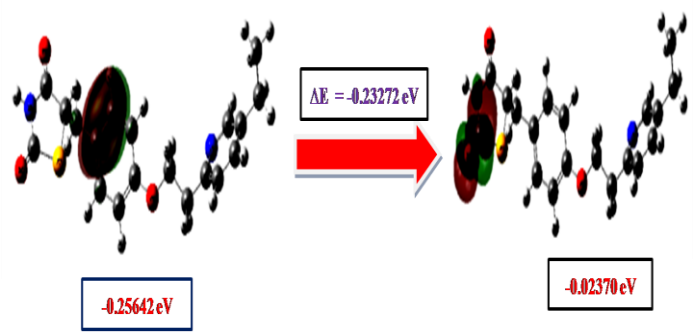

Figure 7 HOMO-LUMO of Pioglitazone.

Molecular docking study

Molecular docking is a powerful approach for predicting the molecular mechanism of protein-ligand interactions. In the present docking study, the Auto Dock suite 4.0 [40-42] has been used to get insight into probable protein-ligand interactions and to identify the binding affinity of the molecules. The docking ligand was got by minimizing its energy at the B3LYP/6-311G++ (d, p) level. Water molecules, as well as co-crystallized agents, were removed using Pymol Software. Lamarckian genetic algorithm (LGA) is used for molecular docking analysis. A particular grid size X is 90Å, Y is 90Å, and Z is 90Å with the aid of the auto grid. The ligand was docked into the functional site of the respective protein and its docking energy was examined to get a minimum value. Docked conformation which has the lowest binding energy with RMSD value 39.795 Å was chosen to investigate the mode of binding. The result is tabulated in **Table 4**. The bond lengths are illustrated in **Figure 8**.

The present structure of Glycogen metabolism (Oryctolagus cuniculus) protein was active with this ligand. The docking position with the lowest docking energy (−7.92 Kcal/mol) is studied. The table shows that the present molecule can dock with the protein 1H5U, a potential antidiabetic drug [43,44], is due to N atom in pyridine ring through 2 hydrogen bonds with lengths 2.5 and 3.1 Å and due to O atoms in the thiazole ring at sites TYR 52, ASN 284, and HIS 341 with bond lengths 2.8, 3.0 and 3.1 Å, respectively.

Table 4 The docking analysis binding pose of Pioglitazone.

Protein ID	Binding energy (kcal/mol)	RMSD (Å)	Bond Residue	Distance (Å)
1H5U	−7.92	38.795	GLU 672	2.5
			TYR 52	2.8
			ASN 284	3.0
			TYR 573	3.1
			HIS 341	3.1

Figure 8 Docking analysis binding pose of Pioglitazone.

Conclusions

The stable conformer of the compound was found at 164° and 311° with their energies at −0.141 Hartree. The structure analysis shows the variation in phenyl ring, ethyl group, methoxy, and thiazolidine group due to the presence of O, S, and N. The bond angle is also varied due to electronic distribution and the hybridization of the carbon atoms in the ring. The charge analysis predicts the change that occurs in C17 and C13 in the phenyl ring, C1, C4, and C5 in the pyridine ring due to the ethyl group and the presence of the N atom. The NMR chemical shift value of C13, C21, and C22 are 177 and 175 ppm because of the attachment of double-bonded O atom and adjacent to N. The vibration analysis results in CH, CS, NH, CO, and CC vibrations. In NBO analysis 7 transitions (1^{st}, 5^{th}, 7^{th} and 8^{th}) are found to be thiazolidine group which shows the n within the ring and double-bonded O outside ring contribute enormously to the electronic property of the molecule. The other 3 transitions are from the pyridine group. All the transitions in the thiazolidine group belong to n-π* transition and those in the pyridine group are π-π* transitions. According to the oscillator strength value, only the 6^{th} transition C2 - C3 to C4 - N9 (27.87 $KJmol^{-1}$) (π-π*) will have the maximum intensity in UV-Visible analysis. HOMO occurs in the phenyl ring and LUMO occurs in the N atom of the thiazole group. The docking proves that the molecule can be used as an antidiabetic agent.

References

[1] J Varshosaz, S Ahmadipour, M Tabbakhian and S Ahmadipour. Nanocrystalization of Pioglitazone by precipitation method. *Drug Res.* 2018; **68**, 576-83.

[2] Y Hu, L Huang, M Shen, Y Liu, G Liu, Y Wu, F Ding, K Ma, W Wang, Y Zhang, Z Shao, X Cai and L Xiong. Pioglitazone protects compression-mediated apoptosis in nucleus pulposus mesenchymal stem cells by suppressing oxidative stress. *Oxid. Med. Cell. Longev.* 2019; **2019**, 4764071.

[3] X Xi, C Zou, Z Ye, Y Huang, T Chen and H Hu. Pioglitazone protects tubular cells against hypoxia / reoxygenation injury through enhancing autophagy via AMPK-mTOR signaling pathway. *Eur. J. Pharmacol.* 2019; **863**, 172695.

[4] N Satheeshkumar, S Shantikumar, R Srinivas, S Shantikumar and R Srinivas. Pioglitazone: A review of analytical methods. *J. Pharm. Anal.* 2014; **4**, 295-302.

[5] V Balaji, V Seshiah, G Ashtalakshmi, SG Ramanan and M Janarthinakani. Brief communication a retrospective study on finding correlation of pioglitazone and incidences of bladder cancer in the Indian population. *Indian J. Endocrinol. Metabol.* 2014; **18**, 425-8.

[6] R Mirza and B Sharma. Beneficial effects of pioglitazone , a selective peroxisome proliferator-activated receptor- γ agonist in prenatal valproic acid-induced behavioral and biochemical autistic like features in Wistar rats. *Int. J. Dev. Neurosci.* 2019; **76**, 6-16.

[7] ME Cam, S Yildiz, H Alenezi, S Cesur, GS Ozcan, G Erdemir, U Edirisinghe, D Akakin, DS Kuruca, L Kabasakal, O Gunduz and M Edirisinghe. Evaluation of burst release and sustained release of pioglitazone-loaded fibrous mats on diabetic wound healing: An *in vitro* and *in vivo* comparison study. *J. R. Soc. Interface* 2020; **17**, 20190712.

[8] C Guizhen, W Jin, S Jingxin, Z Zhilong and Z Litao. Efficacy and safety of pioglitazone for treatment of plaque psoriasis: A systematic review and meta-analysis of randomized controlled trials. *J. Dermatolog. Treat.* 2020; **31**, 680-6.

[9] JZ Zhang, Y Ding, F Xiang, S Yu, D Zhang, M Guan and XJ Kang. Effectiveness and safety of different doses of pioglitazone in psoriasis: A meta-analysis of randomized controlled trials. *Chin. Med. J.* 2020; **133**, 444-51.

[10] RA Defronzo, S Inzucchi, M Abdul-ghani and SE Nissen. Pioglitazone: The forgotten, cost-effective cardioprotective drug for type 2 diabetes. *Diabetes Vasc. Dis. Res.* 2019; **16**, 133-43.

[11] AK Rai and DK Rai. Spectroscopic studies of some antidiabetic drugs. *Spectrochim. Acta Mol. Biomol. Spectros.* 2003; **59**, 1673-80.

[12] T Hosseinnejad and S Mahdavian. Quantum chemistry study on regioselectivity in ruthenium catalyzed synthesis of 1,5-disubstituted 1,2,3-triazoles. *Comput. Theor. Chem.* 2018; **1143**, 29-35.

[13] H Roohi, AR Nowroozi and E Anjomshoa. H-bonded complexes of uracil with parent nitrosamine: A quantum chemical study. *Comput. Theor. Chem.* 2011; **965**, 211-20.

[14] BK Paul and N Guchhait. A quantum chemical computational insight into the intramolecular hydrogen bond interaction in an antibacterial drug molecule-2-acetylindan-1,3-dione. C*omput. Theor. Chem.* 2013; **1012**, 20-6.

[15] AA Starikova, AG Starikov and VI Minkin. Quantum chemical modeling of pyrene-4,5-dione

adducts with cobalt diketonates. *Comput. Theor. Chem.* 2016; **1076**, 74-80.
[16] N Issaoui, H Ghalla, F Bardak, M Karabacak, NA Dlala, HT Flakus and B Oujia. Combined experimental and theoretical studies on the molecular structures, spectroscopy, and inhibitor activity of 3-(2-thienyl)acrylic acid through AIM, NBO,FT-IR, FT-Raman, UV and HOMO-LUMO analyses, and molecular docking. *J. Mol. Struct.* 2017; **1130**, 659-68.
[17] ŽB Milanović, DS Dimić, EH Avdović, DA Milenković, JD Marković, OR Klisurić, SR Trifunović and ZS Marković. Synthesis and comprehensive spectroscopic (X-ray, NMR, FTIR, UV-Vis), quantum chemical and molecular docking investigation of 3-acetyl-4-hydroxy-2-oxo-2H-chromen-7-yl acetate. *J. Mol. Struct.* 2021; **1225**, 129256.
[18] USP Offire, MJS Dewar and GP Ford. *Of the american chemical society*. 1977, 1685-91.
[19] S Banerjee and AK Mukherjee. A detailed quantum chemical study of the interactions of [Pt(dien)Cl] + with a series of S-donor ligands: A computational approach. *Comput. Theor. Chem.* 2012; **991**, 116-23.
[20] K Jayasheela, PB Nagabalasubramanian and S Periandy. Conformational & spectroscopic characterization, charge analysis and molecular docking profiles of chromone-3-carboxylic acid using a quantum hybrid computational method. *Heliyon* 2020; **6**, e04775.
[21] S Segar, K Manivannane and S Periandy. NMR, UV and NBO analysis of aspirin using spectral and computational tools. *NOVIY MIR Res. J.* 2021; **6**, 11-32.
[22] A Sagaama and N Issaoui. Design, molecular docking analysis of an anti-inflammatory drug, computational analysis and intermolecular interactions energy studies of 1-benzothiophene-2-carboxylic acid. *Comput. Biol. Chem.* 2020; **88**, 107348.
[23] J Foresman and A Frisch. *Exploring chemistry with electronic structure methods*. Gaussian, Pittsburgh PA, 1996.
[24] N Sundaraganesan, B Anand, C Meganathan, BD Joshua and H Saleem. Vibrational spectra and assignments of 3-aminobenzyl alcohol by ab initio Hartree-Fock and density functional method. *Spectrochim. Acta Mol. Biomol. Spectros.* 2008; **69**, 198-204.
[25] A Abdel, MS El and AO Abdelhamid. Synthesis and antimicrobial activities of pyrido[2,3-d]pyrimidine, pyridotriazolopyrimidine, triazolopyrimidine, and pyrido[2,3-d:6,5d']dipyrimidine derivatives. *Eur. J. Chem.* 2012; **3**, 455-60.
[26] S Ramalingam, S Periandy and S Mohan. Vibrational spectroscopy (FTIR and FTRaman) investigation using ab initio (HF) and DFT (B3LYP and B3PW91) analysis on the structure of 2-amino pyridine. *Spectrochim. Acta Mol. Biomol. Spectros.* 2010; **77**, 73-81.
[27] V Arjunan, S Mohan, S Subramanian and BT Gowda. Synthesis, fourier transform infrared and Raman spectra, assignments and analysis of N-(phenyl)- and N-(chloro substituted phenyl)-2,2-dichloroacetamides. *Spectrochim. Acta Mol. Biomol. Spectros.* 2004; **60**, 1141-59.
[28] TJ Ajayi and M Shapi. Hirshfeld surface analysis and DFT studies on molecular structure, vibrational spectra, NMR chemical shifts and NBO analysis of Bis(2-hydroxyethyl(phenyl)carbamodithioate) nickel (II). *J. Mol. Struct.* 2019; **1197**, 308-17.
[29] S Aayisha, TSR Devi, S Janani, S Muthu, M Raja and R Hemamalini. Structural (PES), AIM, spectroscopic profiling (FT-IR, FT-Raman, NMR and UV), HOMO-LUMO and docking studies of 2,2-dimethyl-N-(2-pyridinyl)propanamide: A DFT approach. *Chem. Data Collect.* 2019; **24**, 100287.
[30] V Krishnakumar, M Sivasubramanian and S Muthunatesan. Density functional theory study and vibrational analysis of FT-IR and FT-Raman spectra of N-hydroxyphthalimide. *J. Raman Spectrosc.* 2009; **40**, 987-91.
[31] B Chandralekha, R Hemamalini, S Muthu and S Sevvanthi. Spectroscopic (FT-IR, FT-RAMAN, NMR, UV-Vis) investigations, computational analysis and molecular docking study of 5-bromo-2-hydroxy pyrimidine. *J. Mol. Struct.* 2020; **1218**, 128494.
[32] M Asif, H Sajid, F Ullah, S Khan, K Ayub, MA Gilani, M Arshad, MS Akhter and T Mahmood. Quantum chemical study on sensing of NH_3, NF_3, NCl_3 and NBr_3 by using cyclic tetrapyrrole. *Comput. Theor. Chem.* 2021; **1199**, 113221.
[33] A Ganguly, BK Paul, S Ghosh and N Guchhait. A computational acumen into the relative applicability of geometrical and quantum chemical criteria in assessing intramolecular hydrogen bonding (IMHB) interaction: 5-Halosalicylic acids as representative examples. *Comput. Theor. Chem.* 2013; **1018**, 102-14.
[34] SA Siddiqui, T Rasheed and AK Pandey. Quantum chemical study of PtFn and PtCln (n=1-6) complexes: An investigation of superhalogen properties. *Comput. Theor. Chem.* 2012; **979**, 119-27.
[35] RP Gangadharan. Natural Bond Orbital (NBO) population analysis of 1-Azanapthalene-8-ol. *Acta*

Phys Pol. A 2014; **125**, 18-22.
[36] K Govindarasu and E Kavitha. Vibrational spectra, molecular structure, NBO, UV, NMR, first order hyperpolarizability, analysis of 4-Methoxy-4′-Nitrobiphenyl by density functional theory, *Spectrochim. Acta Mol. Biomol. Spectros.* 2014; **122**, 130-41.
[37] H Song, J Gao and L Wu. Fluorouracil drug sensing characteristics of pristine and Al-doped BC_3 nanosheets: Quantum chemical study. *Comput. Theor. Chem.* 2020; **1182**, 112847.
[38] KO Sulaiman and AT Onawole. Quantum chemical evaluation of the corrosion inhibition of novel aromatic hydrazide derivatives on mild steel in hydrochloric acid. *Comput. Theor. Chem.* 2016; **1093**, 73-80.
[39] HP Li, XP Shen, K Han, G Tang and ZH Zhang. Quantum chemistry study on the third-order nonlinear optical properties of spirobifluorene derivatives. *Comput. Theor. Chem.* 2013; **1023**, 95-8.
[40] F Basha A, FLA Khan, S Muthu and M Raja. Computational evaluation on molecular structure (Monomer, Dimer), RDG, ELF, electronic (HOMO-LUMO, MEP) properties, and spectroscopic profiling of 8-Quinolinesulfonamide with molecular docking studies. *Comput. Theor. Chem.* 2021; **1198**, 113169.
[41] MK Chaudhary, A Srivastava, KK Singh, P Tandon and BD Joshi. Computational evaluation on molecular stability, reactivity, and drug potential of frovatriptan from DFT and molecular docking approach. *Comput. Theor. Chem.* 2020; **1191**, 113031.
[42] M Zhang and X Zhu. Computational investigation of flavonol-based GLP-1R agonists using DFT calculations and molecular docking. *Comput. Theor. Chem.* 2020; **1190**, 113005.
[43] American Diabetes Association. Standards of medical care in diabetes-2014. *Diabetes Care* 2014; **37**, 14-80.
[44] S Kalra and N Agrawal. Diabetes and HIV: Current understanding and future perspectives. *Curr. Diabetes Rep.* 2013; **13**, 419-27.